Supplement of Hydrol. Earth Syst. Sci., 30, 1261–1290, 2026
https://doi.org/10.5194/hess-30-1261-2026-supplement

Hydrology and Earth System Sciences
Open Access
EGU

Supplement of

Synergistic impact of simultaneously assimilating radar- and radiometer-based soil moisture retrievals on the performance of numerical weather prediction systems

Yonghwan Kwon et al.

Correspondence to: Yonghwan Kwon (yhkwon@kiaps.org)

S1. KIM hybrid 4DEnVar DA scheme

KIM's 4DEnVar DA system consists of deterministic and stochastic (ensemble) components whose atmospheric analyses are generated using the KIM VARiational DA (KVAR, Song and Kwon, 2015) and four-dimensional local ensemble transform Kalman filter (LETKF, Shin et al., 2016) schemes, respectively. KIM LETKF independently performs analysis updates by assimilating almost the same atmospheric observations as used in the deterministic component (i.e., KVAR), but the main function of LETKF in the KIM DA system is currently to construct ensemble background error covariance of KVAR (Kwon et al., 2018). The relative contribution of the ensemble background error covariance gradually increases from 45% at the poles to 70% at the equator in the troposphere and then gently decreases above the troposphere. Three-dimensional spatial localizations are implemented using the Gaspari and Cohn Gaussian-like localization function (Gaspari and Cohn, 1999). To obtain an appropriate ensemble spread in LETKF, an additive inflation (Shin et al., 2018) and relaxation-to-prior perturbation (Whitaker and Hamill, 2012) are applied together.

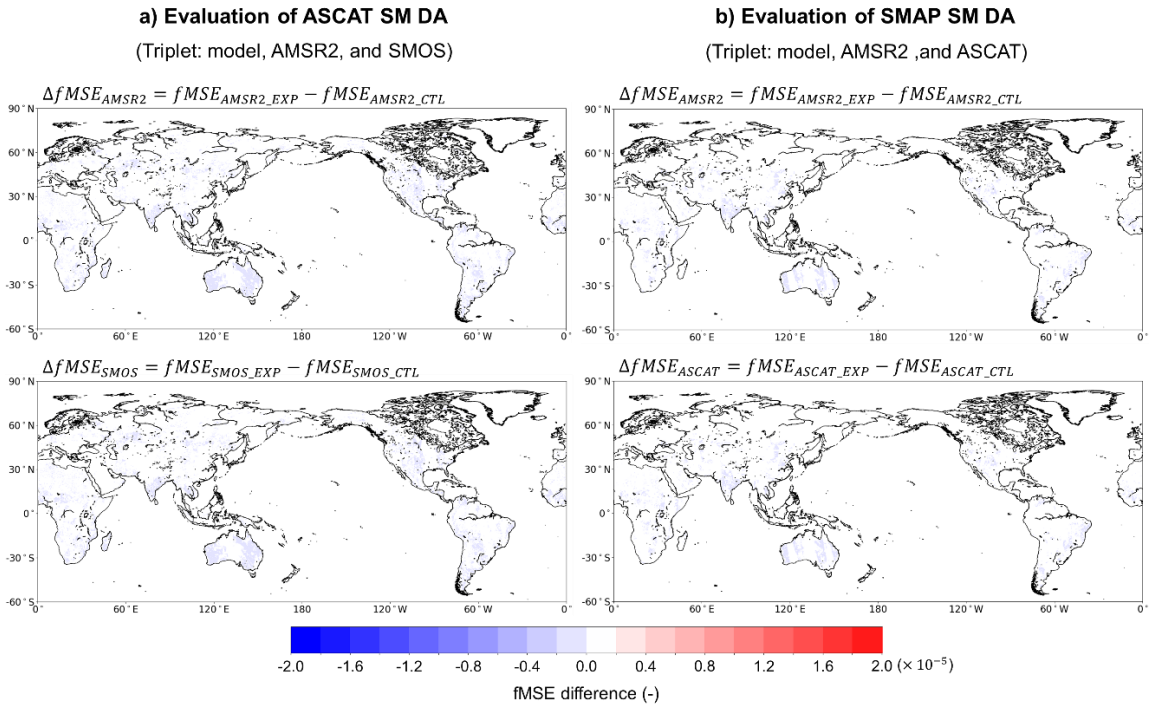

Figure S1. fMSE differences of AMSR2, SMOS, and ASCAT soil moisture data between DA and CTL experiments when used as triplet components to evaluate (a) ASCAT DA (SG_AT) and (b) SMAP DA (SG_SP).

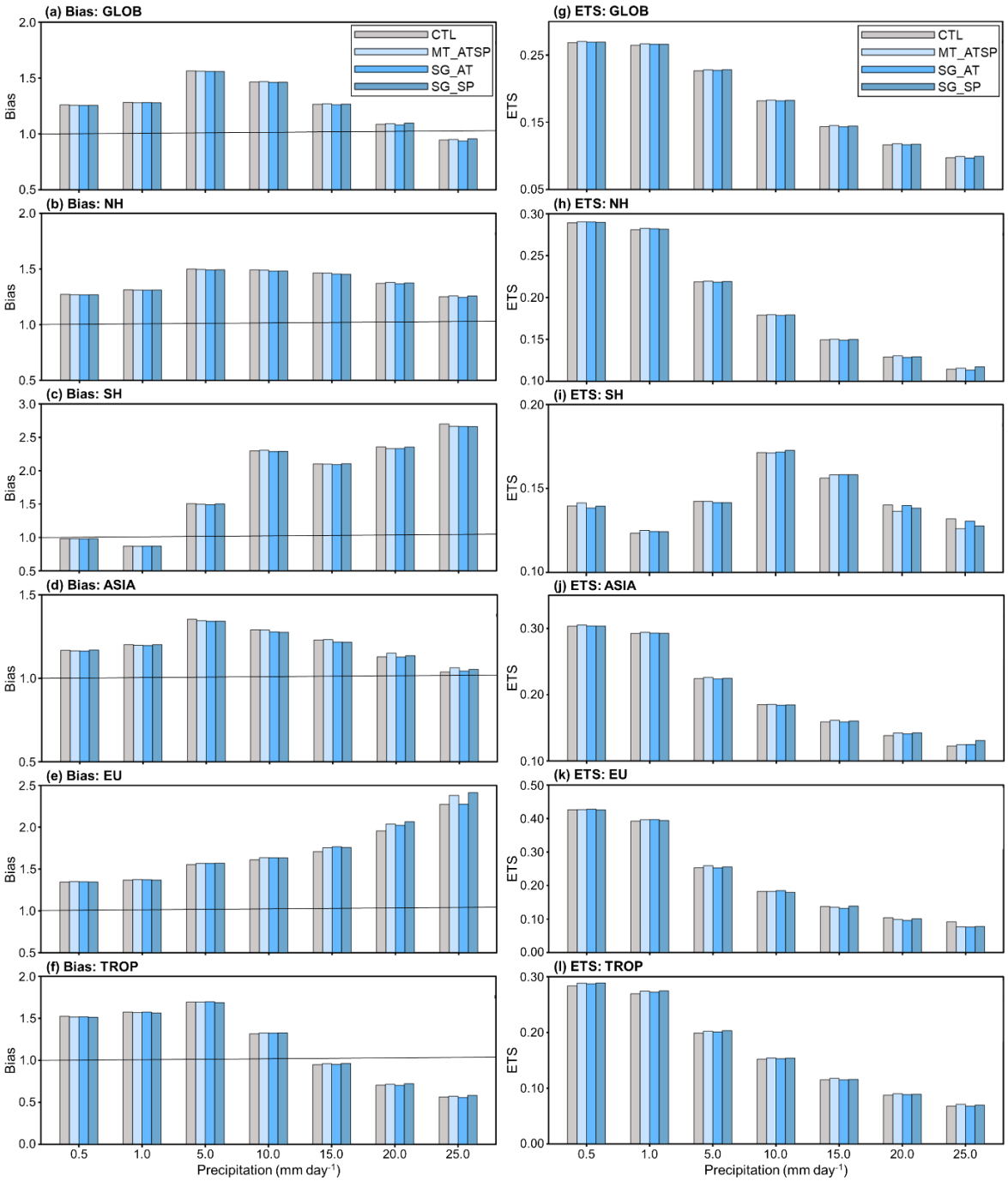

Figure S2. Frequency bias (FB; a to f) and equitable threat score (ETS; g to l), averaged over 24-72 h precipitation forecasts from the 00 UTC cycle in July 2022, for six domains [i.e., global domain (GLOB; a and g), Northern Hemisphere (NH; b and h), Southern Hemisphere (SH; c and i), Asia (ASIA; d and j), Europe (EU; e and k), and tropical area (TROP; f and l)]. The skill metrics are computed for seven conventional thresholds (i.e., 0.5, 1.0, 5.0, 10.0, 15.0, 20.0, and 25.0 mm day^{-1}).

S2. Limitation of the anomaly correction method

The anomaly correction method is based on the critical assumption that systematic differences in higher statistical moments (e.g., standard deviation) between model simulations and observations are negligible compared to those in the climatological SM mean (Kwon et al., 2022). Here, we discuss the limitations of the anomaly-based bias correction approach by applying it to the Soil Moisture and Ocean Salinity (SMOS) SM data assimilation (DA), although the SMOS data are not included in the multi-sensor SM DA explored in this study.

The SMOS L2 SM Neural Network (NN) product (Rodríguez-Fernández et al., 2017) disseminated by the European Space Agency (ESA, https://smos-diss.eo.esa.int/oads/access/) is used. This SM data is generated by applying a NN algorithm that are trained on the SMOS L2 SM retrievals using the SMOS H and V polarized brightness temperature (average ground resolution of 43 km) at incidence angles of 30 to 45° and the European Centre for Medium-Range Weather Forecasts (ECMWF) Integrated Forecast System (IFS) surface soil temperature as inputs. The SMOS L2 SM NN product is provided based on discrete global grid (DGG) systems, and thus the DGG-SM values are assigned to the model grids when the center of SMOS DGG falls within the model latitude-longitude boundaries before assimilation.

Differences in the SM temporal mean and standard deviation between the Noah land surface model (LSM) simulations (without SM DA) and SM retrievals [(from the Soil Moisture Active Passive (SMAP) and SMOS)] are plotted in Figure S3. The figure shows that, compared to SMAP, SMOS exhibits a larger bias from the Noah SM simulation in both the mean and standard deviation. SMOS generally shows a higher SM standard deviation than the Noah LSM. Specifically, the median of the standard deviation difference between SMOS and Noah is -0.019 $m^3 m^{-3}$, whereas it is 0.003 $m^3 m^{-3}$ for SMAP and Noah (Figure S3a). The standard deviation of the SMOS SM temporal variation is much larger than that of the Noah LSM and SMAP SM for most land cover types, except in tundra regions (Figure S3b). Figure S3 indicates that the SMOS SM data and Noah LSM (driven by the KIM forcing) do not satisfy the underlying assumption of the anomaly correction method. Therefore, Figures S4 and S5 show that SMOS DA employing the anomaly correction degrades the 2-m specific humidity and air temperature analysis as compared to the control case (CTL; without SM DA) and SMOS DA case employing the CDF matching.

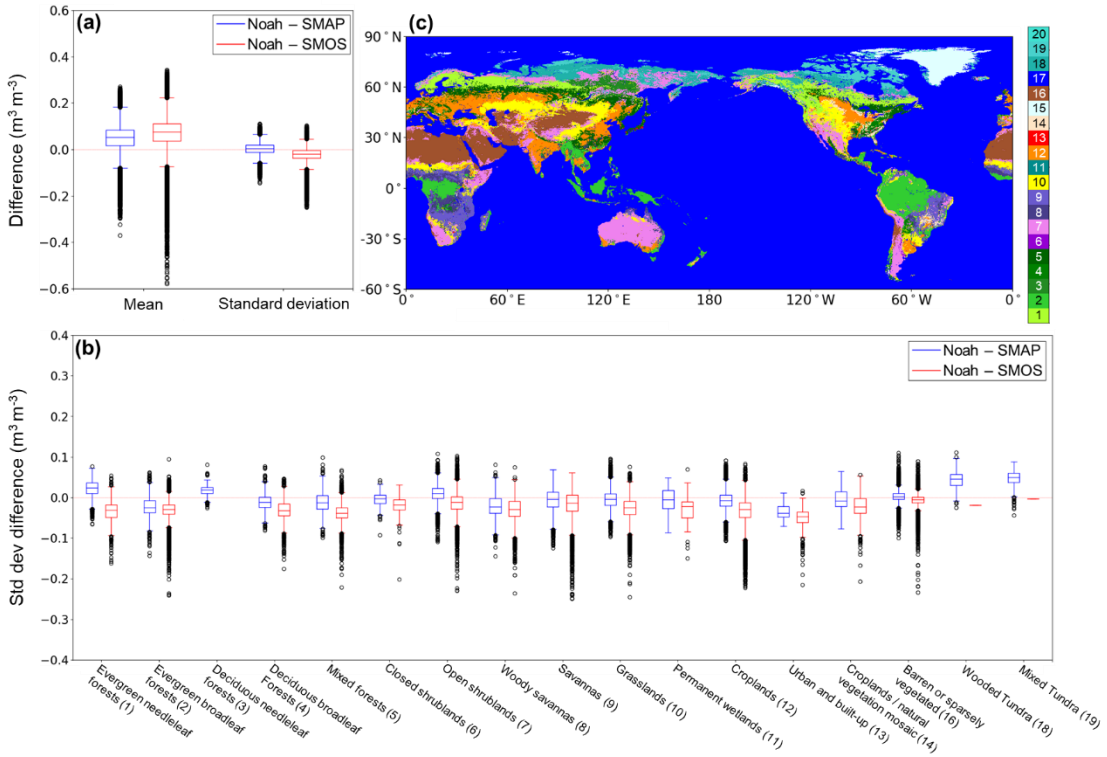

Figure S3. Differences in the mean and standard deviation of the SM estimates between the Noah LSM (without SM assimilation) and satellite-based products (i.e., SMAP and SMOS before bias correction), which are plotted (a) for global grids and (b) for different dominant land-cover types shown in Figure (c). The dominant land-cover types (1: evergreen needleleaf forests, 2: evergreen broadleaf forests, 3: deciduous needleleaf forests, 4: deciduous broadleaf forests, 5: mixed forests, 6: closed shrublands, 7: open shrublands, 8: woody savannas, 9: savannas, 10: grasslands, 11: permanent wetlands, 12: croplands, 13: urban and built-up, 14: croplands/natural vegetation mosaic, 15: snow and ice, 16: barren or sparsely vegetated, 17: water, 18: wooded tundra, 19: mixed tundra, 20: bare ground tundra) are obtained from the Moderate resolution imaging spectroradiometer (MODIS)-based International Geosphere-Biosphere Programme (IGBP) global land-cover classification (Friedl et al., 2002).

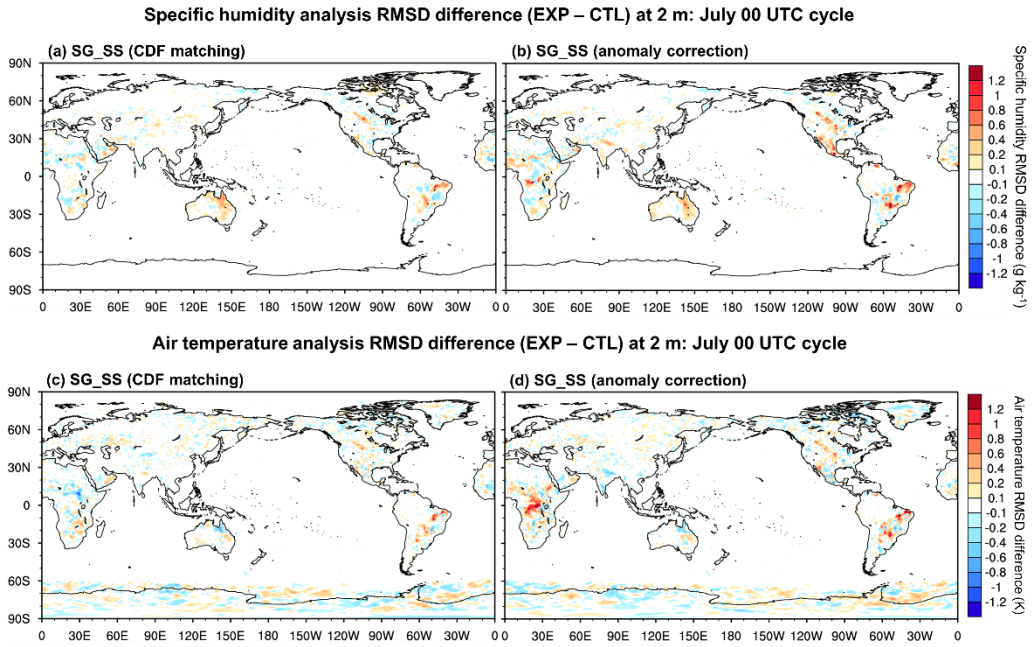

Figure S4. RMSD differences in the 2-m specific humidity analysis (a and b) and 2-m air temperature analysis (c and d) between the SMOS SM DA cases using different bias correction methods [i.e., SG_SS (CDF matching) and SG_SS (anomaly correction)] and CTL (without SM DA) for the July 2022 00 UTC cycle. The European Center for Medium-Range Weather Forecasts (ECMWF) Integrated Forecasting System (IFS) analysis (ECMWF, 2017) is used as reference data.

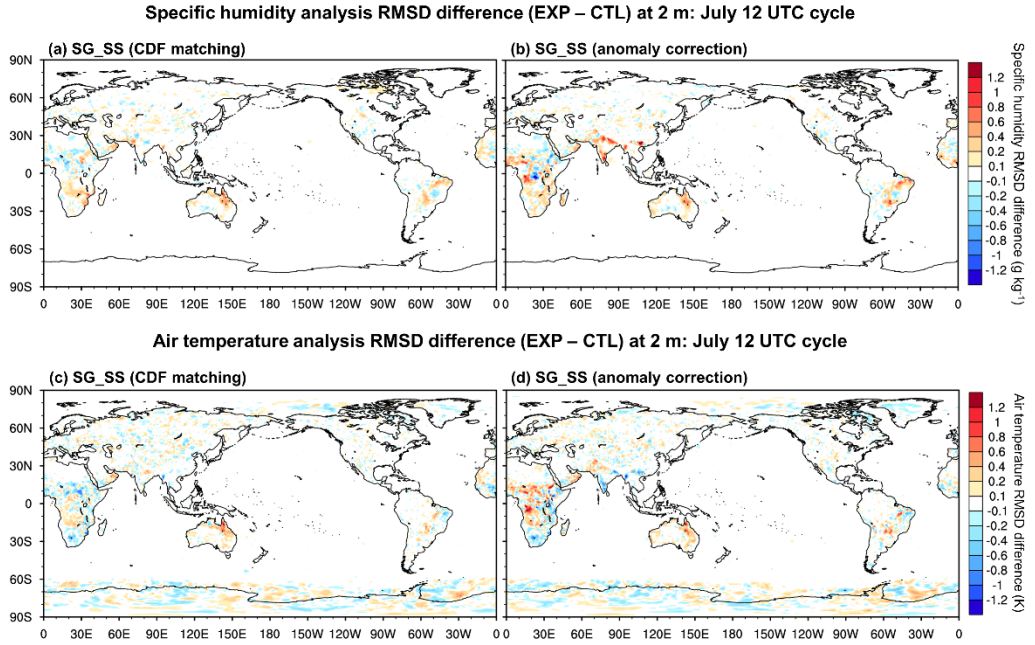

Figure S5. RMSD differences in the 2-m specific humidity analysis (a and b) and 2-m air temperature analysis (c and d) between the SMOS SM DA cases using different bias correction methods [i.e., SG_SS (CDF matching) and SG_SS (anomaly correction)] and CTL (without SM DA) for the July 2022 12 UTC cycle. The European Center for

Medium-Range Weather Forecasts (ECMWF) Integrated Forecasting System (IFS) analysis (ECMWF, 2017) is used as reference data.

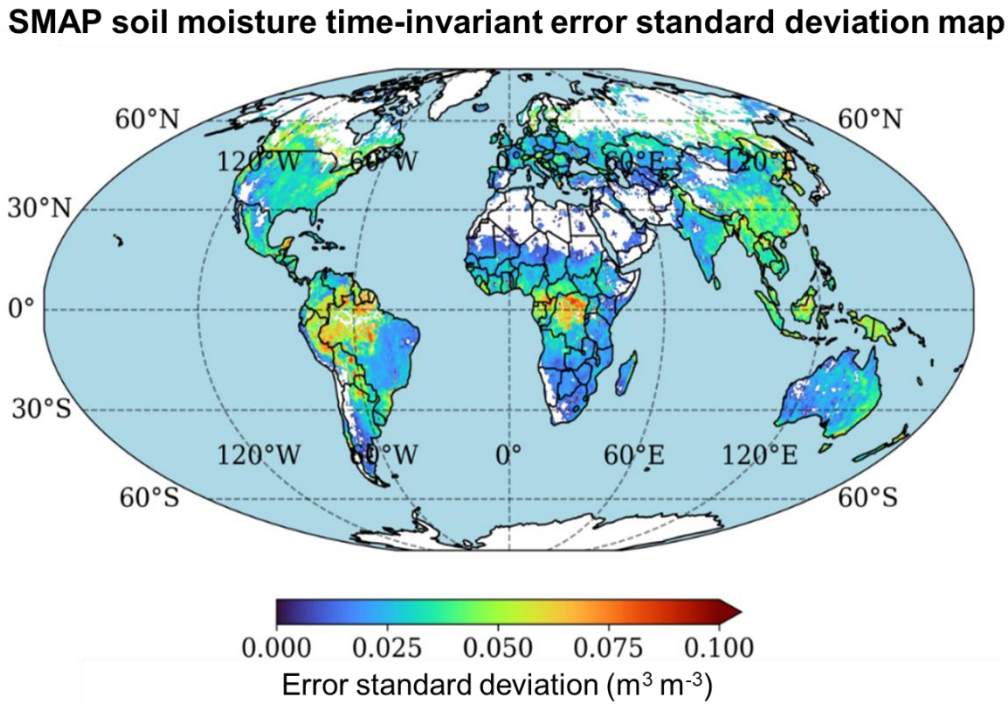

Figure S6. A map of SMAP soil moisture (SM) time-invariant error standard deviations, which has been reproduced from Figure 5 in Kim et al. (2025) with permission.

References

Kim, S., Kim, H., Kwon, Y., and Nguyen, H. H.: A stand-alone framework for predicting spatiotemporal errors in satellite-based soil moisture using tree-based models and deep neural networks, Gisci. Remote Sens., 62, 2475572, https://doi.org/10.1080/15481603.2025.2475572, 2025.

ECMWF: IFS Documentation CY43R3 - Part II: Data assimilation. European Centre for Medium-Range Weather Forecasts, Reading, UK, 103 pp, https://doi.org/10.21957/v61kmv92i, 2017.

Friedl, M. A., McIver, D. K., Hodges, J. C. F., Zhang, X. Y., Muchoney, D., Strahler, A. H., Woodcock, C. E., Gopal, S., Schneider, A., Cooper, A., Baccini, A., Gao, F., and Schaaf, C.: Global land cover mapping from MODIS: algorithms and early results, Remote Sens. Environ., 83, 287–302, https://doi.org/10.1016/S0034-4257(02)00078-0, 2002.

Gaspari, G. and Cohn, S. E.: Construction of correlation functions in two and three dimensions, Q. J. Roy. Meteor. Soc., 125, 723–757, https://doi.org/10.1002/qj.49712555417, 1999.

Kwon, I. -H., Song, H. -J., Ha, J. -H., Chun, H. -W., Kang, J. -H., Lee, S., Lim, S., Jo, Y., Han, H. -J., Jeong, H., Kwon, H. -N., Shin, S., and Kim, T. -H.: Development of an operational hybrid data assimilation system at KIAPS, Asia-Pac. J. Atmos. Sci., 54, 319–335, https://doi.org/10.1007/s13143-018-0029-8, 2018.

Kwon, Y., Kumar, S. V., Navari, M., Mocko, D. M., Kemp, E. M., Wegiel, J. W., Geiger, J. V., and Bindlish, R.: Irrigation characterization improved by the direct use of SMAP soil moisture anomalies within a data assimilation system, Environ. Res. Lett., 17, 084006, https://doi.org/10.1088/1748-9326/ac7f49, 2022.

Rodríguez-Fernández, N. J., Sabater, J. M., Richaume, P., de Rosnay, P., Kerr, Y. H., Albergel, C., Drusch, M., and Mecklenburg, S.: SMOS near-real-time soil moisture product: processor overview and first validation results, Hydrol. Earth Syst. Sci., 21, 5201–5216, https://doi.org/10.5194/hess-21-5201-2017, 2017.

Shin, S., Kang, J. -S., and Jo, Y.: The local ensemble transform Kalman filter (LETKF) with a global NWP model on the cubed sphere, Pure Appl. Geophys., 173, 2555–2570, https://doi.org/10.1007/s00024-016-1269-0, 2016.

Shin, S., Kang, J. -H., Chun, H. -W., Lee, S., Sung, K., Cho, K., Jo, Y., Kim, J. -E., Kwon, I. -H., Lim, S., and Kang, J. -S.: Real data assimilation using the Local Ensemble Transform Kalman Filter (LETKF) system for a global nonhydrostatic NWP model on the cubed-sphere, Asia-Pac. J. Atmos. Sci., 54, 351–360, https://doi.org/10.1007/s13143-018-0022-2, 2018.

Song, H. -J. and Kwon, I. -H.: Spectral transformation using a cubed-sphere grid for a three-dimensional variational data assimilation system, Mon. Weather Rev., 143, 2581–2599, https://doi.org/10.1175/MWR-D-14-00089.1, 2015.

Whitaker, J. S. and Hamill, T. M.: Evaluating methods to account for system errors in ensemble data assimilation, Mon. Weather Rev., 140, 3078–3089, https://doi.org/10.1175/MWR-D-11-00276.1, 2012.